

Decorrelation of participant and spectator angular momenta in heavy-ion collisions

Joseph R. Adams  and Michael A. Lisa 

Department of Physics, Ohio State University, Columbus, Ohio 43210, USA



(Received 22 November 2021; accepted 16 November 2022; published 12 December 2022)

High-energy heavy-ion collisions contain enormous angular momentum, $|\vec{J}|$, which is $O(10^3-10^6\hbar)$ in the range of collision energy, $\sqrt{s_{\text{NN}}}$, spanned experimentally by the Relativistic Heavy Ion Collider (RHIC) and the Large Hadron Collider (LHC). A fraction of \vec{J} is transferred to the overlapping collision region, which is indispensable for measuring observables such as vorticity-driven hadron spin alignment with \hat{J} . Experiments estimate the orientation of \hat{J} of the participant nucleons within the collision overlap region, \hat{J}_{part} , by using that of the forward- and backward-going spectating nucleons \hat{J}_{spec} . Using two models, we study the decorrelation between \hat{J}_{part} and \hat{J}_{spec} , driven both by angular-momentum conservation and event-by-event fluctuations, as well as by the decorrelation between the orientation of the elliptic overlap region and the $\hat{J}_{\text{part}} \cdot \sqrt{s_{\text{NN}}}$ -dependent decorrelation is observed in both of these cases and is large enough to be an important corrective factor used when experimentally observing phenomena driven by \vec{J} .

DOI: [10.1103/PhysRevC.106.064904](https://doi.org/10.1103/PhysRevC.106.064904)

I. INTRODUCTION

Relativistic heavy-ion collisions generate sufficient energy densities to momentarily [$O(1 \text{ fm}/c)$] deconfine constituent quarks, and thereby create the conditions required to study the strong nuclear force described by quantum chromodynamics (QCD). The state of matter produced is the so-called quark-gluon plasma (QGP) [1–5], which has been the subject of intense study for decades; theorists and experimentalists study a variety of phenomena over a wide range of center-of-mass, nucleon-nucleon collision energy, $\sqrt{s_{\text{NN}}}$, in an effort to characterize the QCD phase diagram [6].

Phenomena driven by the angular momentum of participating nucleons within the collision overlap region, \vec{J}_{part} , have been of much interest [7–15]. Experimentally, the orientation of \hat{J}_{part} is not known exactly and must be approximated with the orientation of the angular momentum of the forward- and backward-going spectator nucleons, \hat{J}_{spec} , which are characterized by having a forward rapidity, y , or pseudorapidity, η , with $|y|, |\eta| \gtrsim 1-2$. The QGP state, formed in the collision overlap region, ultimately emits particles across a range of rapidity, but typically only the midrapidity ($|y|, |\eta| \lesssim 1-2$) particles' paths are able to be reconstructed experimentally. Observables such as the spin orientations of hadrons, \vec{S}_{H} , which have been shown to be globally aligned with \hat{J}_{sys} [12–14,16], are therefore only accessible at midrapidity. Ideally, then, the correlation between observables such as \vec{S}_{H} and the angular-momentum orientation of the corresponding midrapidity region, \hat{J}_{mid} , could be studied.

The angular momentum of the system, \vec{J}_{sys} , is perpendicular in the transverse plane (which is orthogonal to the beam axis) to the impact parameter, \vec{b} , connecting the centers of the two nuclei. \hat{J}_{part} instead fluctuates about \hat{J}_{sys} on an event-by-event basis, due to the randomness of nucleon positions

within the colliding nuclei. While the effects of initial-state fluctuations in heavy-ion collisions have been thoroughly investigated [17–29], it has yet to be discussed in the context of decorrelation between \hat{J}_{part} and \hat{J}_{spec} .

Through the use of a simple and intuitive model, we show in this study that the effects of both initial-state fluctuations and angular-momentum conservation lead to a significant decorrelation between the true \hat{J}_{part} and \hat{J}_{part} as estimated by \hat{J}_{spec} . Furthermore, by using a more realistic model, which evolves in time and simulates parton interactions we find a significantly larger suppression of the correlation between \hat{J}_{spec} and the \hat{J}_{mid} that is experimentally of interest. This decorrelation is strongly dependent on $\sqrt{s_{\text{NN}}}$ and would require experimental observations of phenomena driven by angular momentum to correct for this effect. While it may seem natural to attempt to avoid such corrective factors by measuring \hat{J}_{mid} directly from the azimuthal distribution of particles emitted at midrapidity, we find a decorrelation between the orientation of the roughly elliptic shape of the overlap region, practically disallowing such a method.

II. MODELS

The first of two models used to study these effects is a simple Monte Carlo-Glauber (MCG) model [30]. Our MCG model consists of randomly generating angular and radial coordinates according to the Woods-Saxon distribution,

$$\rho(r) = \frac{\rho_0}{1 + e^{\frac{r-R}{a}}}, \quad (1)$$

with the appropriate Jacobians. In this study, we look at ^{197}Au , where $\rho_0 = 0.1693 \text{ fm}^{-3}$, $R = 6.38 \text{ fm}$, and $a = 0.535 \text{ fm}$ [31]. An impact parameter $|\vec{b}|$ is chosen according to $dN/d\vec{b} \propto b$, and two nuclei are generated around two points

a distance b_i from each other before recentering the nuclei to maintain the chosen b . While generating nucleon positions, any newly generated nucleon whose center lies within 0.9 fm of another nucleon's center within the same nucleus is regenerated.

The qualification that a nucleon must satisfy to be considered a participant is that its center must lie within d_\perp of at least one nucleon from the other nucleus. d_\perp is related to the beam energy and the nucleon-nucleon inelastic cross section at that energy, which is parameterized according to [32]:

$$\begin{aligned}\sigma_{\text{NN}}^{\text{total}} &= 48 + 0.522(\ln p)^2 - 4.51 \ln p \\ \sigma_{\text{NN}}^{\text{elastic}} &= 11.9 + 26.9p^{-1.21} + 0.169(\ln p)^2 - 1.85 \ln p \\ d_\perp &= \sqrt{\frac{\sigma_{\text{NN}}^{\text{total}} - \sigma_{\text{NN}}^{\text{elastic}}}{\pi}} = \sqrt{\frac{\sigma_{\text{NN}}^{\text{inelastic}}}{\pi}},\end{aligned}\quad (2)$$

where p is the center-of-mass nucleon momentum. The dependence of d_\perp on $\sqrt{s_{\text{NN}}}$ is weak. For the collision energy $\sqrt{s_{\text{NN}}} = 27$ GeV, somewhat arbitrarily chosen for our calculations, $d_\perp = 0.984$ fm.

A series of typical peripheral collisions using the MCG model at varying b is shown in Fig. 1, where Φ_2 describes the orientation of the collision and is defined in Eq. (4). The directions of \hat{J}_{syst} , shown as magenta (dark gray) arrows, \hat{J}_{part} , shown as the gray (medium gray) arrows, and \hat{J}_{spec} , shown as the green (light gray) arrows, are shown for each collision. \hat{J}_{syst} always points in the $-\hat{y}$ direction while \hat{J}_{part} and \hat{J}_{spec} fluctuate about the $-\hat{y}$ direction and point on opposite sides of \hat{J}_{syst} . While our MCG model calculations serve as a nice baseline for building intuitions, they do not incorporate any time evolution of the system and therefore do not allow us to study the effects of angular-momentum redistribution through particle interactions or to select regions in rapidity.

As angular-momentum-driven phenomena are interested mainly in the QGP phase, we do not want to concern ourselves with late-stage interactions or decays, which will act with a disproportionately large lever arm on the angular momentum of the region. The string-melting version of the a multiphase transport (AMPT) model [33] provides the ideal environment for a study of these angular momentum correlations with a more realistic description, while still allowing the user to ignore late-stage interactions and decays. The user has access to the positions and momenta of the spectators and of the partons at hadronization. Although hadronization will redistribute angular momentum to some degree, this is a subdominant effect.

AMPT uses the heavy-ion jet interaction generator (HIJING) [34] for initial conditions and Zhang's parton cascade (ZPC) [35] for handling partonic interactions. The Lund string fragmentation model is used for hadronization and a relativistic transport (ART) model is used for treating hadronic scatterings. For angular momentum calculations, we are only interested in the state of partons at the moment of hadronization, which is at the end of the ZPC stage.

The input parameters to AMPT, besides $\sqrt{s_{\text{NN}}}$, the range of b , and the number of collisions, are not changed. For MCG and AMPT, 50 K events are generated with $0 \leq b \leq 14$ fm. Only one collision energy is studied in MCG as the only

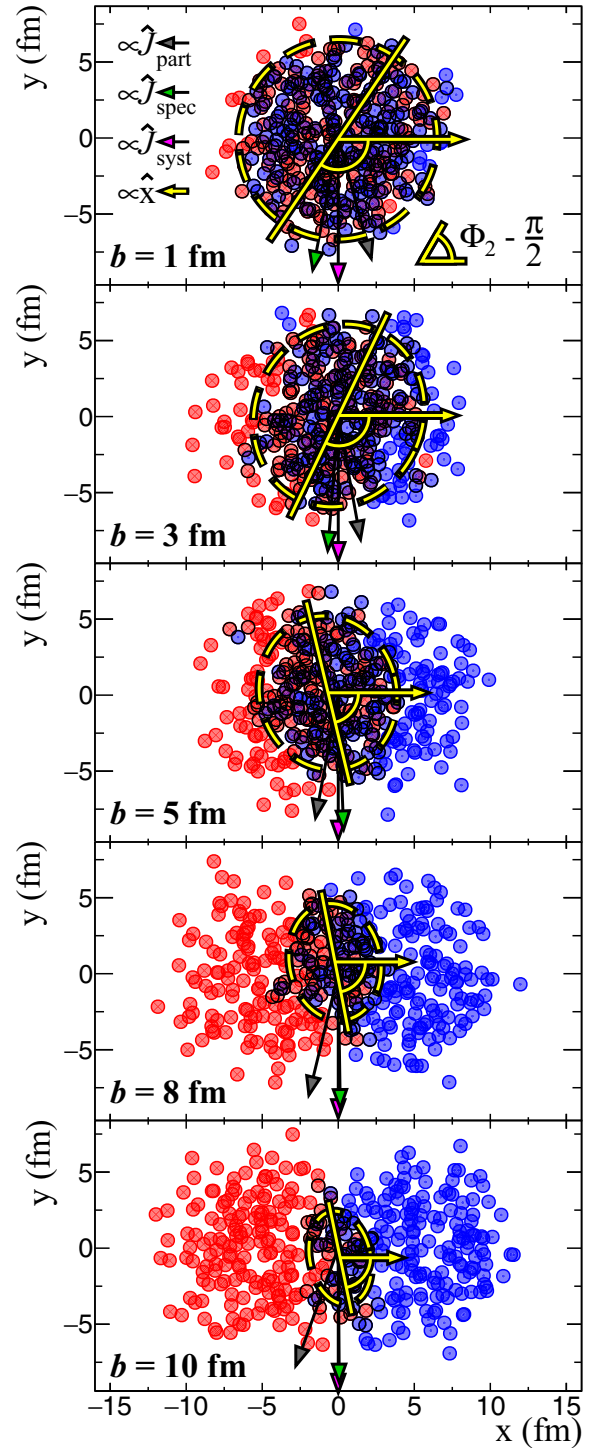


FIG. 1. A series of collisions generated using our MCG model at varying b , viewed in the transverse plane. The participants are outlined in black and the elliptic fit to their positions is displayed in dashed yellow with a line through the major axis. The events shown are typical, in that $\hat{J}_{\text{part}} \cdot \hat{J}_{\text{spec}}|_b \approx \langle \hat{J}_{\text{part}} \cdot \hat{J}_{\text{spec}} \rangle_b$ and $|\sin(\Phi_2)|_b \approx \langle |\sin(\Phi_2)| \rangle_b$.

energy-dependent effect is a slight reduction in r_\perp with $\sqrt{s_{\text{NN}}}$; the somewhat arbitrary choice is $\sqrt{s_{\text{NN}}} = 27$ GeV.

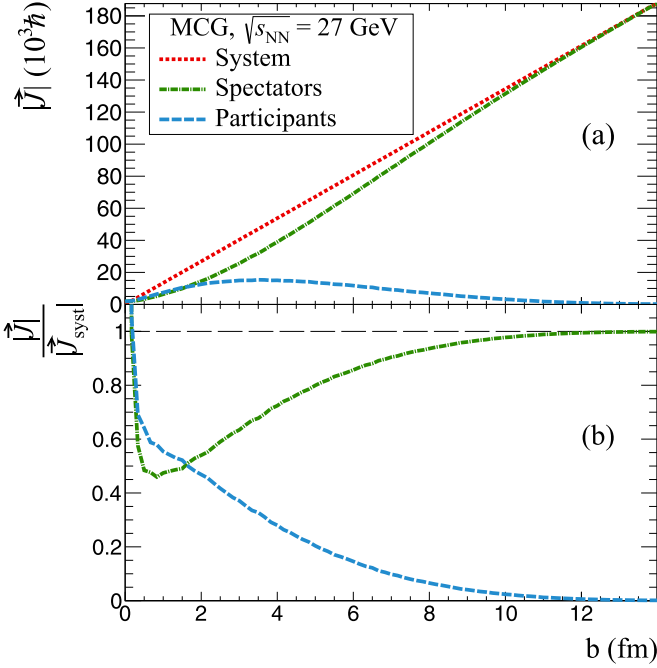


FIG. 2. $|\vec{J}_{\text{part}}|$ is the largest at $b \approx 3.5$ fm, but is sizable for all but peripheral collisions. For very central collisions ($b \lesssim 0.5$ fm), $|\vec{J}_{\text{part}}|$ and $|\vec{J}_{\text{spec}}|$ each become larger than $|\vec{J}_{\text{syst}}|$ since spectators still exist while $|\vec{J}_{\text{syst}}| \rightarrow 0$ as $b \rightarrow 0$.

III. $\vec{J}_{\text{part}}, \vec{J}_{\text{mid}}$ CORRELATIONS WITH $\hat{J}_{\text{syst}}, \hat{J}_{\text{spec}}$

In central heavy-ion collisions ($b \lesssim 3$ fm), $|\vec{J}_{\text{syst}}|$ and $|\vec{J}_{\text{part}}|$ become smaller as $b \rightarrow 0$ while $|\vec{J}_{\text{spec}}|$ remains large; many spectators still exist in these collisions (as seen for example in Fig. 1), which carry a large lever arm. Because of this, $|\vec{J}_{\text{spec}}|$ and $|\vec{J}_{\text{part}}|$ are nonzero even as $b \rightarrow 0$ (see Fig. 2). As $b \rightarrow 0$, \hat{J}_{spec} becomes more random and so, therefore, does \hat{J}_{part} due to conservation of angular momentum. In peripheral collisions ($b \gtrsim 9$ fm) $|\vec{J}_{\text{spec}}|$ dominates the contribution to $|\vec{J}_{\text{syst}}|$ but the effects of initial-state fluctuations on \hat{J}_{spec} diminish as the number of spectators increases, so \hat{J}_{spec} becomes well aligned with \vec{J}_{syst} ; however, the number of participants drops as does the contribution of $|\vec{J}_{\text{part}}|$ to $|\vec{J}_{\text{syst}}|$, so initial-state fluctuations play a significant role in the orientation of \hat{J}_{part} . We might therefore expect \hat{J}_{part} and \hat{J}_{syst} to be poorly correlated in central and peripheral collisions. In midcentral collisions, however, there are enough of both participants and spectators that initial-state fluctuations play a small role in the orientations of \hat{J}_{part} and \hat{J}_{spec} and we might therefore expect them to be well correlated in these collisions. We indeed see this behavior in the solid lines in Fig. 3 measuring $\hat{J}_{\text{part}} \cdot \hat{J}_{\text{syst}}$ with the MCG and AMPT models. Here and henceforth we use the rapidity cut $|y| > 2$ in AMPT to approximately isolate the spectators, as would be done experimentally. When choosing the upper limit of $|y| = 2$ to define the participant region in AMPT, no particles are excluded and we therefore see quite good agreement between the two models.

When instead measuring the correlation between the participants and the spectators, we see that $\hat{J}_{\text{part}} \cdot \hat{J}_{\text{spec}} < \hat{J}_{\text{part}} \cdot$

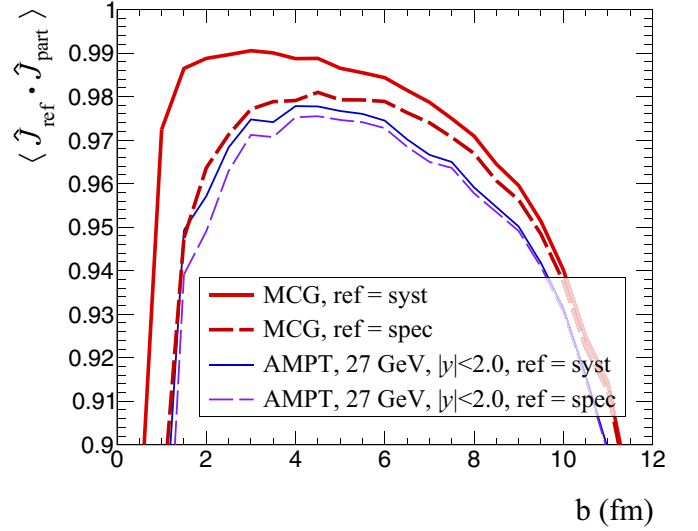


FIG. 3. \hat{J}_{part} and \hat{J}_{syst} are poorly correlated for central and peripheral collisions but are well correlated in between. The correlation between \hat{J}_{part} and \hat{J}_{spec} is smaller than the correlation between \hat{J}_{part} and \hat{J}_{syst} , an effect driven by conservation of angular momentum. In AMPT, shown as the lower two lines, we choose spectators with the somewhat arbitrary cut $|y| > 2$ and in this figure the remaining particles are considered participants.

\hat{J}_{syst} ; this is true both on average as well as event by event, and must be so because of conservation of angular momentum. This is represented in Fig. 1 as a cartoon of midcentral collisions within the MCG model viewed in the transverse plane. By design, $\hat{J}_{\text{syst}} \parallel -\hat{y}$ but initial-state fluctuations will generate a deviation of $\hat{J}_{\text{part}}(\hat{J}_{\text{spec}})$ from $-\hat{y}$ and because of angular-momentum conservation $\hat{J}_{\text{spec}}(\hat{J}_{\text{part}})$ must point along the other side of $-\hat{y}$; i.e., the angle between \hat{J}_{part} and \hat{J}_{spec} must be larger than the angle between \hat{J}_{part} and \hat{J}_{syst} .

Experiments are typically set up to identify particles with tracking at midrapidity (e.g., with time projection chambers) while particle-type-insensitive detectors are placed at forward and backward rapidities to measure particle hits (e.g., with calorimeters). When measuring phenomena driven by angular momentum within the QGP (e.g., global \vec{S}_H alignment with \hat{J}), QGP byproducts are reconstructed at midrapidity while \vec{J}_{spec} is measured using the azimuthal distribution of forward-/backward-going particles as an approximation of \vec{J}_{part} ; however, such an approximation is subject not only to the effects seen in Fig. 3 but also to the experimental constraints of incomplete detector coverage and imperfect detector efficiencies. Because of this limitation, random fluctuations will play a larger role and we might expect the correlation between \hat{J}_{spec} and \hat{J}_{mid} to be smaller than the correlation between \hat{J}_{spec} and \hat{J}_{part} . This effect is shown in Fig. 4 within the AMPT model. For midcentral collisions, \hat{J}_{mid} is well aligned with \hat{J}_{syst} when considering $|y| < 2$; however, the degree of alignment drops substantially when considering the region $|y| < 1$ typically used in experimental studies. This is striking; if taken at face value, this would translate to a correction of roughly 25% on the observable of interest.

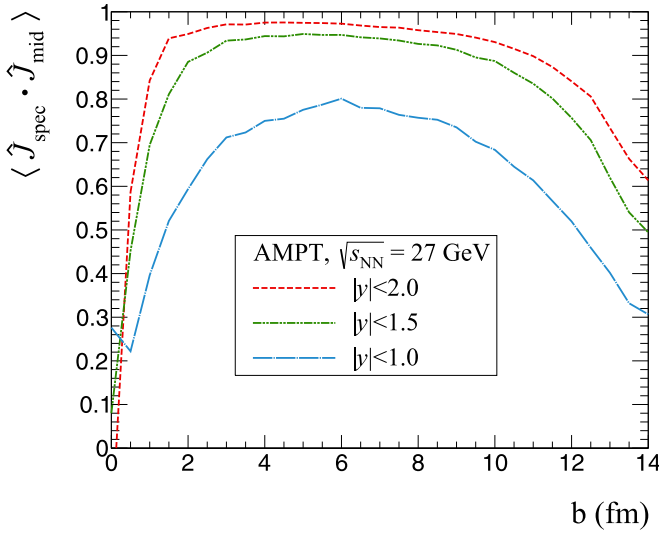


FIG. 4. The correlation between \hat{J}_{mid} and \hat{J}_{spec} becomes smaller as we further constrain the size of the rapidity window used for the calculation of \hat{J}_{mid} where initial-state fluctuations play a larger role. Experiments typically are limited to $|y| < 1$. Recall that $|y| = 2$ is our participant-spectator cutoff in AMPT, so that $\bar{J}_{\text{mid},|y|<2} = \bar{J}_{\text{part}}$.

At larger collision energies, the fraction of emitted particles that lie in the rapidity window $|y| < 1$ becomes smaller; we might therefore expect the correlator $\langle \hat{J}_{\text{mid}} \cdot \hat{J}_{\text{spec}} \rangle$ to become smaller with increasing $\sqrt{s_{\text{NN}}}$. On the other hand, the fraction of emitted particles that lie in the spectator (forward) rapidity region becomes larger and will impact \hat{J}_{spec} . In Fig. 5 we see that, despite this, $\langle \hat{J}_{\text{mid}} \cdot \hat{J}_{\text{spec}} \rangle$ becomes smaller as

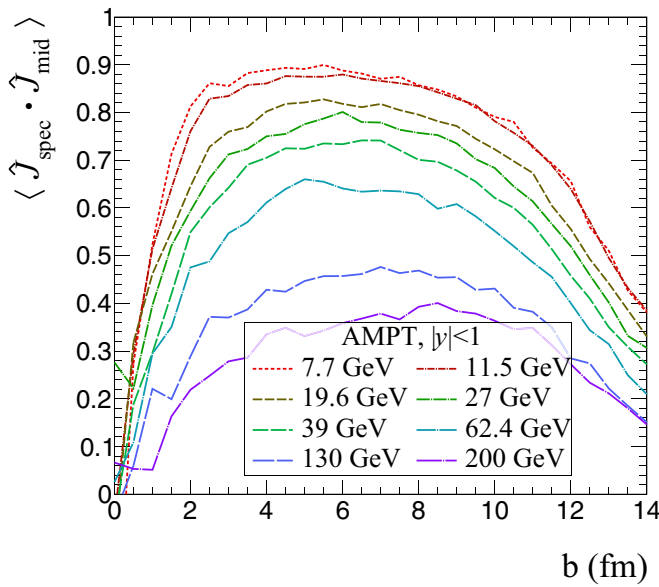


FIG. 5. The correlation between \hat{J}_{mid} and \hat{J}_{spec} becomes smaller as we increase $\sqrt{s_{\text{NN}}}$, where a given rapidity window includes a smaller fraction of emitted particles and initial-state fluctuations play a larger role. This is similar to the effects driving the observation in Fig. 4. The values of $\sqrt{s_{\text{NN}}}$ are chosen to match those of the RHIC Beam Energy Scan (BES).

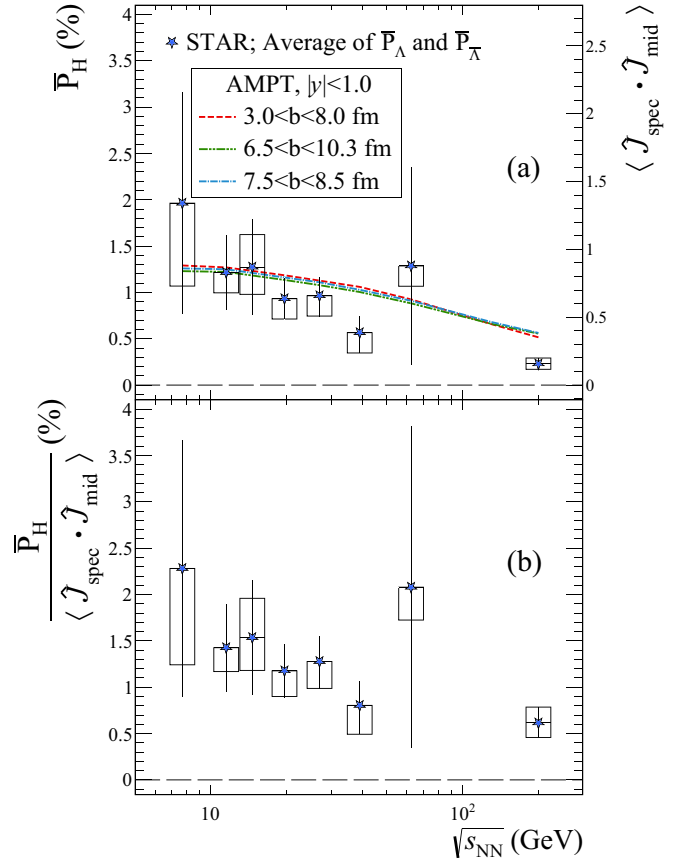


FIG. 6. (a) shows that the correlation between \hat{J}_{mid} and \hat{J}_{spec} for midcentral collisions (the event class used when studying angular-momentum-driven phenomena) falls with $\sqrt{s_{\text{NN}}}$. $3 < b < 8$ fm describes the region from Fig. 5 where the correlation is flat, and $6.5 < b < 10.3$ fm and $7.5 < b < 8.5$ fm are two ways of approximating 20–50 % central collisions. Experimental results of global hyperon polarization [11,12,36], \bar{P}_H , are shown alongside these calculations. Also shown, in (b) are these results scaled by the relevant correlation calculated with AMPT.

$\sqrt{s_{\text{NN}}}$ becomes larger. This correlation depends strongly on $\sqrt{s_{\text{NN}}}$, differing by more than a factor of 2 between the lowest and highest collision energies. In Fig. 6, $\langle \hat{J}_{\text{mid}} \cdot \hat{J}_{\text{spec}} \rangle$ is shown for midcentral collisions, defined in a number of ways that yield very similar results, as a function of $\sqrt{s_{\text{NN}}}$. Any $\sqrt{s_{\text{NN}}}$ -dependent experimental observable driven by angular momentum within the QGP would be corrected in such a manner, by $\langle \hat{J}_{\text{mid}} \cdot \hat{J}_{\text{spec}} \rangle^{-1}$. Similarly, it is important for model predictions to use \hat{J}_{part} or \hat{J}_{mid} , rather than \hat{J}_{sys} , when calculating phenomena driven by angular momentum within the QGP.

The global spin polarization of hyperons, \bar{P}_H , is one such observable that would require correction, and experimental measurements of \bar{P}_H [11,12,36] are shown alongside the correlator $\langle \hat{J}_{\text{mid}} \cdot \hat{J}_{\text{spec}} \rangle$ in Fig. 6. Both \bar{P}_H and $\langle \hat{J}_{\text{mid}} \cdot \hat{J}_{\text{spec}} \rangle$ fall with increasing $\sqrt{s_{\text{NN}}}$, though \bar{P}_H demonstrates a stronger dependence. The ratio of \bar{P}_H to $\langle \hat{J}_{\text{mid}} \cdot \hat{J}_{\text{spec}} \rangle$ is shown in the bottom panel of Fig. 6; the scaled \bar{P}_H demonstrates a notably weaker dependence on $\sqrt{s_{\text{NN}}}$. In practice, a more detailed

study, specific to a detector's coverage and acceptance or to a model's assumptions, would need to be performed to apply a correction. Without performing such corrections, there will be an apparent dependence on $\sqrt{s_{\text{NN}}}$ driven at least in part by the behavior observed in Fig. 6.

IV. $\hat{J}_{\text{part}}, \hat{J}_{\text{mid}}$ CORRELATIONS WITH GEOMETRY

The overlap region of a heavy-ion collision is roughly elliptic on average, with the major axis of the ellipse somewhat aligned with \hat{y} . We can fit the participant coordinates to an ellipse in order to determine its orientation and study the correlation between \hat{J}_{part} and this orientation. We characterize the initial shape through harmonic-eccentricity coefficients ε_n and event-plane angles Φ_n [37]:

$$\varepsilon_n e^{in\Phi_n} = -\frac{\int r dr d\phi r^n e^{in\phi} e(r, \phi)}{\int r dr d\phi r^n e(r, \phi)}. \quad (3)$$

By taking $n = 2$ and treating the initial energy-density distribution $e(r, \phi)$ as a sum of δ functions, each at the position of a nucleon, this reduces to

$$\Phi_2 = \frac{1}{2} \left[\arctan \frac{\sum_i r_{\perp,i}^2 \sin(2\phi_i)}{\sum_i r_{\perp,i}^2 \cos(2\phi_i)} + \pi \right], \quad (4)$$

where r_{\perp} and ϕ are the polar coordinates of the participant nucleons in the transverse plane, as measured from the center of mass of the participants. This procedure is only applicable in the MCG model where all nucleons are either considered to be participants or spectators. In the AMPT model, we can reconstruct the orientation of the elliptic overlap region responsible for the midrapidity region by taking advantage of elliptic flow; the pressure gradient is larger along the shorter axis of the ellipse than it is along the longer axis. Because of this, the azimuthal distribution of emitted particles in a rapidity window will reveal the orientation of the relevant overlap region [38]:

$$\Phi_2 = \frac{1}{2} \text{atan2} \left(\sum_i w_i \sin(2\phi_i), \sum_i w_i \cos(2\phi_i) \right), \quad (5)$$

where the weight, w_i , is typically the transverse momentum, p_T .

For central collisions, the overlap region is quite circular and for very peripheral collisions only a small number of nucleons participate; in both cases, initial-state fluctuations play a large role in the orientation of the elliptic fit and therefore on Φ_2 . In midcentral collisions, the overlap region is sufficiently elliptic and there are enough participants that initial-state fluctuations will be subdominant; we might therefore expect Φ_2 to be best aligned with $\phi_{\hat{J}_{\text{syst}}} \pm \pi/2$ for midcentral collisions. Such behavior is apparent in the solid lines in Fig. 7.

We might also intuitively make the naïve assumption that the somewhat elliptic participant region would be spinning about its major axis and therefore expect better alignment between Φ_2 and $\phi_{\hat{J}_{\text{part}}}, \phi_{\hat{J}_{\text{mid}}}$ than between Φ_2 and $\phi_{\hat{J}_{\text{syst}}}$. If this were true, then the problematic suppression of $\hat{J}_{\text{mid}} \cdot \hat{J}_{\text{spec}}$ discussed in Sec. III could potentially be avoided by measuring \hat{J}_{mid} directly from Φ_2 ; however, when considering again

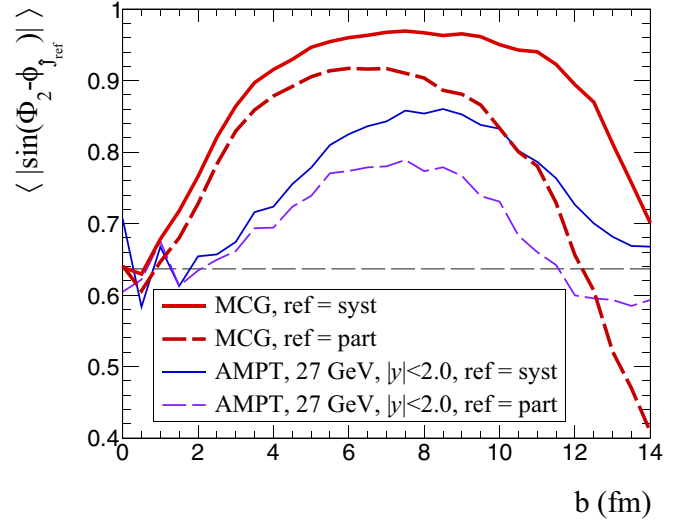


FIG. 7. The correlation between the orientation of the elliptic overlap region and \hat{J}_{syst} is largest for midcentral collisions, in line with expectations. Counterintuitively, however, there is a suppressed correlation between the orientation of the ellipse and \hat{J}_{part} . The absolute value of $\sin(\Phi_2 - \phi_{\hat{J}_{\text{part}}})$ is used since Φ_2 is physically indistinguishable from $\Phi_2 \pm \pi$. Recall that $|y| = 2$ is our participant-spectator cutoff in AMPT, shown as the lower two lines, so that $\hat{J}_{\text{mid}, |y| < 2} = \hat{J}_{\text{part}}$. The horizontal dashed line represents $2/\pi$, which is the average absolute value of the sine of the difference between two random, uncorrelated numbers.

Fig. 7, there is apparently a significant suppression of the correlation between Φ_2 and $\phi_{\hat{J}_{\text{part}}}, \phi_{\hat{J}_{\text{mid}}}$. This can be understood by dividing a given tilted elliptic overlap region in two, lengthwise, and considering that one half is dominated by positive-rapidity nucleons while the other is dominated by negative-rapidity nucleons. By applying the right-hand rule to these two halves it is clear that \hat{J}_{part} will tilt to the left as the elliptic overlap region tilts to the right, and vice versa. One can see in Fig. 1 a few examples of the major axis tilting away from \hat{J}_{part} over a range of b .

For the same reasons that we expected $\hat{J}_{\text{mid}} \cdot \hat{J}_{\text{spec}}$ to decrease both when reducing the size of the window in y and when increasing $\sqrt{s_{\text{NN}}}$, we might expect the correlation $\langle |\sin(\Phi_2 - \phi_{\hat{J}_{\text{mid}}})| \rangle$ to again decrease in AMPT when considering $|y| < 1$, as well as when considering larger $\sqrt{s_{\text{NN}}}$. While not shown in this paper, we indeed did find such additional suppressions to this correlation. This decorrelation between Φ_2 and $\phi_{\hat{J}_{\text{part}}}, \phi_{\hat{J}_{\text{mid}}}$ demonstrates that one can not avoid the corrective factors discussed in Sec. III by indirectly measuring \hat{J}_{mid} through Φ_2 .

V. SUMMARY

Initial-state fluctuations drive a decorrelation between \hat{J}_{syst} and $\hat{J}_{\text{part}}, \hat{J}_{\text{mid}}$, which is the largest for central and peripheral collisions. Conservation of angular momentum further suppresses this correlation between \hat{J}_{spec} and $\hat{J}_{\text{part}}, \hat{J}_{\text{mid}}$, albeit slightly. Only \hat{J}_{spec} is experimentally accessible, and is used as an approximation of \hat{J}_{mid} . As the size of the

midrapidity window becomes smaller, the correlation between \hat{J}_{spec} and \hat{J}_{mid} is suppressed further. Similarly, this decorrelation becomes more dramatic with increasing $\sqrt{s_{\text{NN}}}$.

The orientation of the elliptic overlap region, Φ_2 , has a smaller correlation with $\hat{J}_{\text{part}}, \hat{J}_{\text{mid}}$ than with \hat{J}_{sys} , in conflict with potentially intuitive expectations. The correlation between the orientation of elliptic shape and \hat{J}_{part} is further suppressed when constraining the midrapidity window to $|y| < 1$, as well as when increasing $\sqrt{s_{\text{NN}}}$. Deducing \hat{J}_{part} from Φ_2 is therefore not a viable method to avoid the problems of correlation suppression between \hat{J}_{mid} and \hat{J}_{spec} .

The findings presented here hold significant implications for measurements of phenomena driven by angular momentum within the QGP, and particularly for those interested in the

dependence on $\sqrt{s_{\text{NN}}}$. Based on our model-dependent study, it is crucial for studies of angular-momentum-driven phenomena, such as experimental measurements of \bar{P}_H , to correct for the decorrelation between \hat{J}_{spec} and \hat{J}_{mid} in a $\sqrt{s_{\text{NN}}}$ -dependent manner, and for model predictions of such phenomena to use \hat{J}_{mid} instead of \hat{J}_{sys} . Without these corrections, any observed dependence will be driven at least in part by this decorrelation.

ACKNOWLEDGMENTS

We thank Jinfeng Liao and Giorgio Torrieri for helpful conversations. This work was supported by the U.S. Department of Energy Grant No. DE-SC0020651.

-
- [1] E. V. Shuryak, *Phys. Rep.* **61**, 71 (1980).
 - [2] J. Adams *et al.* (STAR Collaboration), *Nucl. Phys. A* **757**, 102 (2005).
 - [3] K. Adcox *et al.* (PHENIX Collaboration), *Nucl. Phys. A* **757**, 184 (2005).
 - [4] B. B. Back *et al.* (PHOBOS Collaboration), *Nucl. Phys. A* **757**, 28 (2005).
 - [5] I. Arsene *et al.* (BRAHMS Collaboration), *Nucl. Phys. A* **757**, 1 (2005).
 - [6] Y. Akiba *et al.*, [arXiv:1502.02730](https://arxiv.org/abs/1502.02730) [nucl-ex]
 - [7] F. Becattini and M. A. Lisa, *Annu. Rev. Nucl. Part. Sci.* **70**, 395 (2020).
 - [8] Z.-T. Liang and X.-N. Wang, *Phys. Rev. Lett.* **94**, 102301 (2005); Erratum: **96**, 039901(E) (2006).
 - [9] F. Becattini and F. Piccinini, *J. Phys. G: Nucl. Part. Phys.* **35**, 104013 (2008).
 - [10] B. Betz, M. Gyulassy, and G. Torrieri, *Phys. Rev. C* **76**, 044901 (2007).
 - [11] B. I. Abelev *et al.* (STAR Collaboration), *Phys. Rev. C* **76**, 024915 (2007); Erratum: **95**, 039906(E) (2017).
 - [12] L. Adamczyk *et al.* (STAR Collaboration), *Nature (London)* **548**, 62 (2017).
 - [13] S. Acharya *et al.* (ALICE Collaboration), *Phys. Rev. C* **101**, 044611 (2020).
 - [14] J. Adam *et al.* (STAR Collaboration), *Phys. Rev. Lett.* **126**, 162301 (2021).
 - [15] Y. Jiang, Z.-W. Lin, and J. Liao, *Phys. Rev. C* **94**, 044910 (2016); Erratum: **95**, 049904(E) (2017).
 - [16] M. S. Abdallah *et al.* (STAR Collaboration), *Phys. Rev. C* **104**, L061901 (2021).
 - [17] B. Alver and G. Roland, *Phys. Rev. C* **81**, 054905 (2010); Erratum: **82**, 039903(E) (2010).
 - [18] A. Bzdak and V. Skokov, *Phys. Lett. B* **710**, 171 (2012).
 - [19] J. Błoczyński, X.-G. Huang, X. Zhang, and J. Liao, *Phys. Lett. B* **718**, 1529 (2013).
 - [20] V. Vovchenko, D. Anchishkin, and L. P. Csernai, *Phys. Rev. C* **88**, 014901 (2013).
 - [21] G.-Y. Qin, H. Petersen, S. A. Bass, and B. Müller, *Phys. Rev. C* **82**, 064903 (2010).
 - [22] R. A. Lacey, R. Wei, J. Jia, N. N. Ajitanand, J. M. Alexander, and A. Taranenko, *Phys. Rev. C* **83**, 044902 (2011).
 - [23] J. Qian and U. Heinz, *Phys. Rev. C* **94**, 024910 (2016).
 - [24] J. Jia, *J. Phys. G: Nucl. Part. Phys.* **41**, 124003 (2014).
 - [25] M. Luzum and H. Petersen, *J. Phys. G: Nucl. Part. Phys.* **41**, 063102 (2014).
 - [26] N. Magdy, X. Sun, Z. Ye, O. Evdokimov, and R. Lacey, *Universe* **6**, 146 (2020).
 - [27] F. G. Gardim, G. Giacalone, M. Luzum, and J.-Y. Ollitrault, *Nucl. Phys. A* **1005**, 121999 (2021).
 - [28] R. S. Bhalerao, G. Giacalone, P. Guerrero-Rodríguez, M. Luzum, C. Marquet, and J.-Y. Ollitrault, *Acta Phys. Pol. B* **50**, 1165 (2019).
 - [29] L. Ma, G. L. Ma, and Y. G. Ma, *Phys. Rev. C* **94**, 044915 (2016).
 - [30] M. L. Miller, K. Reygers, S. J. Sanders, and P. Steinberg, *Annu. Rev. Nucl. Part. Sci.* **57**, 205 (2007).
 - [31] G. Fricke and K. Heilig, Nuclear charge radii 79-au gold: Datasheet from *Landolt-Börnstein - group i elementary particles, nuclei and atoms nuclear charge radii in Springer Materials* (Springer-Verlag, Berlin, 2004).
 - [32] L. Montanet, K. Gieselmann, R. M. Barnett, D. E. Groom, T. G. Trippe, C. G. Wohl, B. Armstrong, G. S. Wagman, H. Murayama, J. Stone, J. J. Hernandez, F. C. Porter, R. J. Morrison, A. Manohar, M. Aguilar-Benitez, C. Caso, P. Lantero, R. L. Crawford, M. Roos, N. A. Tornqvist, K. G. Hayes, G. Hohler, S. Kawabata, D. M. Manley, K. Olive, R. E. Shrock, S. Eidelman, R. H. Schindler, A. Gurtu, K. Hikasa, G. Conforto, R. L. Workman, C. Grab, (Particle Data Group), *Phys. Rev. D* **50**, 1173 (1994).
 - [33] Z.-W. Lin, C. M. Ko, B.-A. Li, B. Zhang, and S. Pal, *Phys. Rev. C* **72**, 064901 (2005).
 - [34] M. Gyulassy and X.-N. Wang, *Comput. Phys. Commun.* **83**, 307 (1994).
 - [35] B. Zhang, *Comput. Phys. Commun.* **109**, 193 (1998).
 - [36] J. Adam *et al.* (STAR Collaboration), *Phys. Rev. C* **98**, 014910 (2018).
 - [37] Z. Qiu and U. Heinz, *Phys. Lett. B* **717**, 261 (2012).
 - [38] S. A. Voloshin, A. M. Poskanzer, and R. Snellings, *Landolt-Börnstein* **23**, 293 (2010).